Electron-positron Jets Associated with the Quasar 3C 279

J. F. C. Wardle, D. C. Homan, R. Ojha, and D. H. Roberts

Department of Physics, Brandeis University, Waltham, Massachusetts 02254, USA

Appeared in Nature (1998) vol 395, pg. 457

A long outstanding problem in extragalactic astrophysics is the composition of the relativistic jets of plasma streaming from the nuclei of quasars and active galaxies – whether it is predominantly a "normal" (electron - proton) plasma, or a "pair" (electron - positron) plasma. Distinguishing between these possibilities is crucial for understanding the physical processes occuring close to the putative supermassive black holes in galactic nuclei that create the jets. Here we present a new approach to the problem of jet composition, by detecting circularly polarized radio emission from the archtypal quasar 3C 279, using the VLBA. The circular polarization is produced by Faraday conversion, which requires that the energy distribution of the radiating particles extends to very low energies, indicating that electron – positron pairs are a major component of the jet plasma. Similar detections in three other radio sources, suggest that in general, extragalactic radio jets are composed primarily of an electron – positron plasma.

The most luminous objects in the universe are distant quasars and active galactic nuclei. A few percent of these emit strongly at radio wavelengths, and are powered by twin jets of plasma streaming at close to the speed of light from the nucleus of the underlying galaxy[1]. The central engine in the nucleus is widely believed to be a supermassive black hole of some $10^8 - 10^9$ solar masses[2]. At radio wavelengths the jets are visible from parsec to kiloparsec scales, emitting synchrotron radiation from ultra-relativistic electrons gyrating in a magnetic field. The bulk kinetic energy carried by the jets powers the extended lobes of radio emission far outside the parent galaxy, while synchrotron and inverse Compton emission from the base of the jets generates radiation at optical, x-ray and even gamma ray wavelengths[3,4]. The composition of the jet plasma has been an outstanding issue ever since their discovery. The two main candidates are a "normal" plasma consisting of protons and relativistic electrons (an $e - p$ jet), and a "pair plasma" consisting only of relativistic electrons and positrons (an $e^+ - e^-$ jet).

Electrons and positrons emit synchrotron radiation of identical spectrum and linear polarization, so distinguishing whether the radiating particles are mainly electrons or a mixture of electrons and positrons is difficult. Two lines of argument shed light on the problem. The first comes from matching the total energy flux carried by the jet to the total dissipation observed in electromagnetic radiation, the energy stored in the extended radio lobes in magnetic fields and relativistic particles, and the mechanical work done against the surrounding medium[5,6]. The energy distribution of the radiating particles is assumed to be a power law, $n(\gamma) \propto \gamma^{-(2\alpha+1)}$ for $\gamma_{min} < \gamma < \gamma_{max}$, where $\gamma = (1 - v^2/c^2)^{-\frac{1}{2}}$ is the Lorentz factor of the particle, and α is the observed spectral index of the synchrotron radiation. For an $e - p$ jet, the energy distribution must cut off at $\gamma_{min} \approx 100$, or the jet may carry several orders of magnitude more energy than is seen to be dissipated. For an $e^+ - e^-$ jet, the energy distribution must extend to low energies, $\gamma_{min} \approx 1$, in order that the jet carries sufficient energy. The second line of argument is based on the strong fractional

linear polarization often observed in the jets on parsec scales[7,8]. This strongly limits the amount of internal Faraday rotation (due mainly to the lowest energy electrons) in the jet. Interestingly, the result is similar. For an $e-p$ jet, $\gamma_{min} \geq 100$, while for an $e^+ - e^-$ jet there is no Faraday rotation (since electrons and positrons gyrate in opposite directions) and hence there is no constraint on γ_{min}.

Thus a value of $\gamma_{min} \ll 100$ would be strong evidence in favor of an $e^+ - e^-$ jet, while $\gamma_{min} \geq 100$ would require an $e-p$ jet. The lowest energy radiating particles are not directly observable, because their radiation is strongly self-absorbed, though the signature of a low energy cutoff may be visible in inverse Compton scattered radiation at x-ray and gamma ray wavelengths. Here we present an entirely new approach to the problem of jet composition, by imaging the *circularly* polarized component of the synchrotron emission. We have detected circular polarization from the archtypal violently variable quasar 3C 279, at several epochs, using the Very Long Baseline Array (VLBA) at 15 GHz. We argue that the circular polarization is produced by Faraday conversion[9,10] of linear to circular polarization in the jet plasma, and requires that the energy distribution of the radiating particles extends to $\gamma_{min} \ll 100$, implying an electron - positron jet.

The quasar 3C 279, at a redshift of[11] $z = 0.538$, is one of the most luminous objects in the sky from radio to gamma ray wavelengths, and is violently variable across the electromagnetic spectrum[12,13]. At radio wavelengths, VLBI images[14,15,16] show a bright unresolved core and a one-sided jet which extends to kiloparsec scales[17], ending in diffuse emission. It was the first source in which superluminal motions in the jet were observed[18], and subsequent observations have measured apparent velocities from 4 to 15 times the speed of light (we assume $H_0 = 70$ km s^{-1} Mpc^{-1}, $q_0 = 0.05$). Superluminal motion indicates both bulk relativistic speeds in the jet, and that it makes a small angle to the line of sight. It follows that the observed radiation from the jet at all wavelengths is strongly boosted by

the Doppler effect. Its high flux density in all wavebands makes 3C 279 one of the most extensively observed of all quasars, and a prime laboratory for the study of the physics of extragalactic jets.

The observations

The observations were part of a program to monitor the structure and polarization of 12 rapidly variable compact radio sources, using the VLBA at 22 GHz (λ1.3cm) and 15 GHz (λ2.0cm). Observations were made at intervals of two months, and the consistency between images made at different epochs is an important check on our results. Here we present the July 1996 15 GHz observations of 3C 279. In the **Methods** section at the end of this article, we outline our techniques and some of the tests and simulations we have carried out. We will present elsewhere the the observations of 3C 279 at other epochs, and of the sources 3C 84, 3C 273, and J0530+135, in which we also detected circular polarization.

Images of 3C 279 in total intensity, linear polarization and circular polarization are presented in Figure 1. At a redshift of 0.538, 1 mas corresponds to a linear scale of 5.9 pc.

FIGURES 1a,b,c HERE

Figure 1c shows the circularly polarized image. The circular polarization emitting region is in the core, slightly displaced to the west, and has an integrated flux density of $V = +89 \pm 10$ mJy. Compared to the noise level on the rest of the image, this is a 40σ detection, confirmed by several independent calibration techniques and diagnostic tests (see **Methods**), and it is seen at every epoch for which we have good data.

TABLE 1 HERE

The measured component properties are listed in Table 1. The two components in the core region, CE and CW, probably represent regions of a quasi-continuous inhomogeneous jet, as described by Blandford & Königl [19]. We interpret CE as the optically thick base of

the jet, and CW as being close to the optical surface ($\tau \simeq 1$), possibly enhanced by a newly emerging component. Assuming that the circularly polarized signal is associated with component CW (the higher opacity of CE strongly depresses any circular polarization), its fractional circular polarization is $m_C = +1.0 \pm 0.2\%$. At 22 GHz, the data are significantly noisier due to tropospheric fluctuations and beam squint problems. The "zero V self calibration" and "phase only mapping" techniques (see **Methods**) both show no circularly polarized signal above 50 mJy, corresponding to a fractional polarization of CW at 22 GHz of $m_C \leq 0.5\%$.

The absolute polarization position angle calibration was determined by setting the position angles for component K1 equal to 67° (parallel to the jet direction) at both 15 and 22 GHz. This is consistent with the calibration determined by comparing the VLBA observations of OJ 287 with nearly simultaneous VLA observations. The polarization position angles of CW imply that there is $8° \pm 3°$ of Faraday rotation between 15 and 22 GHz (also observed at other epochs). This corresponds to a Faraday depth at 15 GHz of $\tau_F = -1.1 \pm 0.4$ (observed rotation measure $= -700 \pm 260$ rad m^{-2}). This is an important constraint on the line of sight component of the magnetic field, and is crucial for the interpretation of the circular polarization.

Interpretation

For simplicity, we shall treat CW as a single homogeneous region in the jet, and assume that the optically thin spectral index of CW has the canonical value $\alpha = 0.5$. Our results are not qualitatively different if another value is used. Both the spectrum and the linear polarizations for CW listed in Table 1 are best fit by an optical depth at 15 GHz of about $\tau \approx 0.7$ over a range of magnetic field models, and we shall fix the optical depth at this value. Then, given the observed brightness temperature, we can derive the magnetic field strength using standard formulae[20]. Model fitting gives the size of CW as (0.34 mas)×(< 0.1

mas), elongated along the jet, and we parameterize the transverse size of CW as 0.1η mas. If the opening angle of the jet is taken from components K1 and K2, then the transverse dimension is 0.01 mas (*i.e.* $\eta = 0.1$), and we consider this to be a lower limit on η. We find that $B_\perp = 5.8\eta^2\delta$ mG, where $B_\perp$ is the root-mean-square value of the magnetic field in the plane of the sky, and $\delta = [\gamma_{jet}(1 - \beta_{jet}\cos\theta)]^{-1}$ is the Doppler factor of the radiating fluid (the jet speed is $\beta_{jet}c$, $\gamma_{jet} = (1 - \beta_{jet}^2)^{-\frac{1}{2}}$ is its Lorentz factor, and θ is the inclination of the jet to the line of sight). A synchrotron self-Compton calculation[21] gives $\delta \sim 20$, while the observed proper motion of K1 requires $\delta > 8$. These two estimates bracket a plausible range for δ. The average Lorentz factor of electrons radiating at an observed frequency of 15.36 GHz is $\gamma = 1.2 \times 10^3/\eta\delta$.

To interpret the circular polarization, we must also assume a structure for the magnetic field, and this is strongly constrained by the observed linear polarization. A plausible family of field structures is given by the "shock in jet" models[22,23,24], in which a shock compresses the jet fluid, partially ordering the magnetic field transverse to the jet direction. The linear polarization of the jet (Fig 1b) shows that the electric vectors are generally aligned with the jet direction, indicating a predominantly transverse magnetic field. This is consistent with a shock model, but our results do not depend on this. It is simply a convenient way to describe a general magnetic field structure that contains both a uniform component and a partially ordered tangled component.

The production and transfer of circular polarized radiation (in a uniform magnetic field) is analysed in detail by Jones & O'Dell[9], who give the general solution for the four Stokes parameters at arbitrary optical and Faraday depths. We have written a program to simulate the magnetic field structure described by shock models, and apply their solutions (corrected for typographical errors[23]) cell-by-cell to calculate all four emerging Stokes parameters. The numerical results discussed below are derived from this program.

Intrinsic circular polarization?

Synchrotron radiation has a small intrinsic component of circular polarization[25]. In a uniform magnetic field, the maximum fractional circular polarization at frequency ν is $|m_C| \approx 1/\gamma$, where γ is the Lorentz factor of electrons radiating at ν. More generally, we can write $m_C = -1.6\,\Lambda\,(\nu/\nu_{B\perp})^{-\frac{1}{2}}(B_u/B_\perp)\tan\epsilon$, where B_u is the uniform component of the magnetic field, $B_\perp$ is the r.m.s. value of the magnetic field in the plane of the sky, $\nu_{B\perp} = eB_\perp/2\pi mc$ is the electron gyro frequency, and ϵ is the angle between the jet normal and the line of sight in the frame of the emitting fluid ($\cos\epsilon = \delta\sin\theta$). The factor Λ accounts for the reduction in circular polarization if there are reversals in direction of B_u, and if the charges of the radiating particles are not all the same sign. Defining $f_B = |\int B_u\,dl|/\int |B_u|\,dl$, and $f_C = (n^- - n^+)/(n^- + n^+)$, where n^- and n^+ are the electron and positron densities respectively, then $\Lambda = f_B f_C$. The Faraday depth is also reduced by the same factor. In a real jet, even if the component of magnetic field parallel to the jet is unidirectional at its base ($f_B \sim 1$), it will decay faster with radius ($\propto r^{-2}$) than the transverse field components ($\propto r^{-1}$). Further down the jet, the parallel component of field is likely to be dominated by sheared loops of field[1] and f_B (and hence Λ) is almost certainly small.

Since the Lorentz factor of the electrons radiating at 15 GHz is $\gamma = 1.2\times10^3/\eta\delta$, it is marginally possible to produce the observed circular polarization by this mechanism, but only if the uniform component of magnetic field is unidirectional, $f_B \approx 1$, which we consider physically implausible. Equally important, the numerical simulations show that the fractional circular polarization at 22 GHz should be higher than at 15 GHz by a factor of about 1.14. This is because of the significant opacity at 15 GHz combined with the rather flat ($m_C \propto \nu^{-\frac{1}{2}}$) spectrum of intrinsic circular polarization. This predicts a circularly polarized flux at 22 GHz of 116 mJy, while the data give an upper limit of about 50 mJy. The argument is only slightly weaker for the inhomogeneous jet model[19],

for which it is easily shown that $m_C \propto \nu^0$ (including opacity). For these reasons we reject intrinsic circular polarization as the origin of the observed signal. Faraday conversion of linear polarization to circular polarization, which we consider next, has the advantage of producing an intrinsically much steeper circular polarization spectrum ($m_C \propto \nu^{-3}$ at high frequencies[7]).

Circular polarization from Faraday conversion

A less well known but equally important mechanism for generating circular polarization is Faraday conversion[9,10]. This is based on the fact that the normal modes for radiative transfer in an anisotropic plasma are not purely circular (which leads to Faraday rotation), but slightly elliptical. The small component of linear birefringence converts Stokes parameter U to V, and *vice versa*. Both rotation and conversion are caused by the lowest energy relativistic electrons, and therefore serve as a probe of the low energy end of the electron energy distribution, which is otherwise unobservable. An important difference between them is that Faraday rotation is proportional to the electron gyro frequency, $\nu_{B\perp} = eB_\perp/2\pi mc$, and hence to the sign of the charge on the electrons, while Faraday conversion is proportional to $\nu_{B\perp}^2$. Thus an equal mixture of electrons and positrons can produce Faraday conversion, but not rotation. Indeed, this is a possible observational signature of such a plasma.

It is also important to note that Faraday conversion acts on Stokes U, while the synchrotron mechanism produces only Stokes Q. Stokes U can be produced stochastically by a tangled field, or, more efficiently, by Faraday rotation, which we observe to be present in component CW. At small optical and Faraday depths, the fractional circular polarization produced by conversion is $m_C \approx \frac{1}{6}\tau_F\tau_C m_L^2$, where τ_F and τ_C are the Faraday depth and "conversion depth" respectively, and m_L is the fractional linear polarization. For a power law distribution of electron Lorentz factors, $n(\gamma) \propto \gamma^{-2}$ (corresponding to $\alpha = 0.5$), with a

low energy cutoff at $\gamma = \gamma_{min}$, τ_F and τ_C can be written as[9]

$$\begin{aligned} \tau_F &\approx 1.27\,\tau\,\Lambda\left(\frac{\gamma}{\gamma_{min}}\right)^2 \frac{\ln\gamma_{min}}{\gamma_{min}}\frac{B_u}{B_\perp}\sin\epsilon \\ \tau_C &= -0.96\,\tau\ln(\gamma/\gamma_{min}) \end{aligned}$$

where γ is the Lorentz factor of the radiating electrons.

We have explored numerically a large number of shock models to find combinations of τ_C, γ_{min} and Λ that reproduce the observed linear and circular polarization ($m_L = 9.9 \pm 1.0\%, \tau_F = 1.1 \pm 0.4, m_C = 1.0 \pm 0.2\%$). Table 2 lists the parameters of two such models, representing shocks of different strengths. In both cases, $\Lambda = 1.0$ is formally permitted, giving the largest allowed value of γ_{min}. We have been unable to find an acceptable model in which γ_{min} is greater than 20. The condition $\Lambda = 1$ would require that the uniform magnetic field component, B_u, is also *unidirectional*, which we consider implausible for the reasons stated above. It is far more likely that $\Lambda < 1$ and $\gamma_{min} < 20$. In fact it is entirely possible that $\Lambda \ll 1$ and that γ_{min} approaches unity, though the precise value of γ_l should not be taken too seriously, since the abrupt cutoff is artificial.

TABLE 2 HERE

The energy flux of the jet

As outlined in the introduction, value of $\gamma_{min} < 20$ is strong evidence that the jet plasma is dominated by electron - positron pairs. The total energy flux carried by a relativistic jet can be written as[26]

$$F_E = 4\pi r_{jet}^2 p_{jet}\gamma_{jet}^2\beta_{jet}c(1 + \frac{\gamma_{jet}-1}{\gamma_{jet}}R)$$

where r_{jet} is the jet radius and p_{jet} is the total pressure. The factor $R = \rho c^2/4p_{jet}$ is the ratio of cold matter energy density to pressure, and can be written as $R = 3(1 + 1836 f_C)/16\gamma_{min}\ln(\gamma_{max}/\gamma_{min})$. A lower bound on F_E is found by assuming equipartition between the particles and the field, leading to $F_E \geq 2.5 \times 10^{45}(1 + R)$ erg/sec.

Even if f_C and hence R are small, this is sufficient to power the extended (unbeamed) radio emission[17], and also to produce the (presumed beamed) core radio, optical and gamma ray emission[13], if the Doppler factor is greater than $\delta \simeq 10$. Thus an electron - positron jet in 3C 279 roughly matches the total observed dissipation, while an electron - proton jet exceeds it by one to two orders of magnitude.

Discussion and Conclusions

Reynolds *et al.* [6] present strong arguments that the well known jet in M87 is most likely an electron - positron jet; they also suggest that perhaps Fanaroff - Riley[27] type I (low luminosity) jets are electron - positron jets and FR II (high luminosity) jets may be electron - proton jets. We note that 3C 279 (and also 3C 273 and PKS 0530+138) are high luminosity (type II) jets, while 3C 84 is a low luminosity (type I) jet, suggesting that in general, extragalactic jets may be primarily electron - positron jets.

Both detailed numerical simulations of relativistic jets[28] and simple arguments based on ram-pressure confinement[29] show that jet densities must be extremely low ($\ll$ external density) in order to create the large diffuse lobes seen in FR II sources. This also suggests light, pair dominated jets[30].

If this is the case, it points towards photon cascade[31,32] or pion decay[33,34] processes as the origin of the majority of the radiating particles, which in turn gives valuable clues to the physical mechanisms close to the central black hole that create, collimate and accelerate the jets[1,35].

Methods

The VLBA is equipped with circularly polarized feeds, right (R) and left (L), at each antenna. To measure circular polarization (V) with the VLBA, we must take the difference between two large quantities, $RR = I + V$ and $LL = I - V$, and we are therefore critically sensitive to gain errors.

Fringe fitting, calibration, and imaging in total intensity and linear polarization were carried out using standard techniques[16,36,37] with the software packages AIPS and DIFMAP. It is important that the polarization leakage (D) terms[36] at each antenna be accurately determined and removed from the RR and LL data because they induce *non-closing* errors that are not removed by self-calibration and could mimic a circularly polarized signal.

We have devised three different methods of making images to detect circular polarization, that mitigate to some extent the sensitivity to gain errors.

"Zero V self-calibration": The first and simplest approach is to assume there is no circularly polarized signal from the source of interest and self-calibrate with the assumption $RR = \tilde{I}_{model}$ and $LL = \tilde{I}_{model}$. This essentially forces the strongest peak in the image to appear unpolarized, and if there is no circularly polarized signal in the data, none will be induced by this procedure. For an unequal point double, resembling 3C 279, circular polarization located on the strong core component will be transfered to the weak component *at the same fractional level and with the reversed sign*, while circular polarization originating in the weak component itself will remain largely unchanged.

"Phase-only mapping": A signature of a true circularly polarized signal in a resolved source is a difference between the RR and LL closure phases. In phase-only mapping[38], we set the RR and LL fringe amplitudes equal to unity, but preserve their phases. For an unequal double source, this produces an *antisymmetric* fractional circular polarization image with half of the circularly polarized signal appearing at the position of the weaker component, and half (with opposite sign) at the corresponding position on the opposite side of the phase center. The advantage of this is that it is almost independent of the amplitude calibration, and demonstrates that the circularly polarized signal is indeed present in the closure phases, which are preserved throughout the self-calibration procedure.

"Transfer of gains": The third approach depends on the excellent gain stability of the

VLBA, and can resolve whether the circularly polarized signal is located on the core or in the jet. (In Homan *et al.* [39] we incorrectly associated the circularly polarized signal with component K1.) We assume that the amplitude gain *ratio* of the R and L channels at each antenna is stable over several hours and can be determined from the data on other sources in the observing run (which are interweaved with the observations of 3C 279) and applied to the target source. The image shown in Figure 1 and the results in Table 1 are derived from this approach. For 3C 279, the three methods give consistent results, and we are confident of the reality of the circularly polarized signal, and that it is in fact located in the core region.

We have run many tests and simulations on our observations and calibration techniques, to confirm the reality of our results. The circular polarization signal is present in all frequency channels and cannot be attributed to the behaviour of a single antenna. This was demonstrated by repeating the entire calibration procedure (post-fringe fit) for each IF channel separately, and omitting each antenna in turn from the array. We checked the effect of incorrect subtraction of the antenna D terms from the parallel hand data by simply omitting the correction altogether. This increased the noise on the V image but did not generate a significant spurious circularly polarized component.

Finally, we created three model sources, similar to 3C 279 in I and P structure, with no initial V, V on the core, and V on the jet component. These models contained thermal noise, D-term leakage, time-dependent complex gains, and baseline-based errors. We carried these models through our standard (post fringe-fit) calibration procedure and found that we were able to detect a circularly polarized signal placed in the model data. Equally important, we were unable to generate a V signal when the model contained no V.

1 Begelman, M. C., Blandford, R. D. & Rees, M. J. Theory of extragalactic radio sources. *Rev. Mod. Phys.* **56,** 255-351 (1984).

2 Rees, M. J. Black hole models for active galactic nuclei. *Ann. Rev. Astron. Astrophys.* **22,** 471-506 (1984).

3 Königl A. Relativistic jets as x-ray and gamma ray sources. *Astrophys. J.* **243,** 700-709 (1981).

4 Sikora. M., Begelman, M. C. & Rees, M. J. Comptonization of diffuse ambient radiation by a relativistic jet. The source of gamma rays from blazars? *Astrophys. J.* **421,** 153-162 (1994).

5 Celotti, A. & Fabian, A. C. The kinematic power and luminosity of parsecscale radio jets - an argument for heavy jets. *Mon. Not. R. Astron. Soc.* **264,** 228-236 (1993).

6 Reynolds, C. S., Fabian, A. C., Celotti, A. & Rees, M. J. The matter content of the jet in M87: evidence for an electron-positron jet. *Mon. Not. R. Astron. Soc.* **283,** 873-880 (1996).

7 Wardle, J. F. C. Upper limits on the Faraday rotation in variable radio sources. *Nature* **269,** 563-566 (1977).

8 Jones, T. W. & O'Dell, S. L. Physical conditions in polarized compact radio sources. *Astron & Astrophys* **61,** 291-293 (1977).

9 Jones, T. W. & O'Dell, S. L. Transfer of polarized radiation in self-absorbed synchrotron sources. I - Results for a homogeneous source. *Astrophys. J.* **214,** 522-539 (1977).

10 Jones, T. W. Polarization as a probe of magnetic field and plasma properties of compact radio sources. *Astrophys. J.* **332,** 678-695 (1988).

11 Burbidge. E. M. & Rosenburg, F. D. The redshift of the quasi-stellar radio source

3C 279. *Astrophys. J.* **142,** 1673-1674 (1965).

12 Wehrle, A. *et al.* Multiwavelength observations of a dramatic high-energy flare in the blazar 3C 279. *Astrophys. J.* **497,** 178-187 (1998).

13 Hartman, R. C. *et al.* Simultaneous multiwavelength spectrum and variability of 3C 279 from 10^9 Hz to 10^{24} Hz. *Astrophys. J.* **461,** 698-712 (1996).

14 Unwin, S. C., Cohen, M. H., Biretta, J. A., Hodges, M. W. & Zensus, J. A. Superluminal motion in the quasar 3C 279. *Astrophys. J.* **340,** 117-128 (1989).

15 Carrara, E. A., Abraham, Z., Unwin, S. C. & Zensus, J. A. The milliarcsecond structure of the quasar 3C 279. *Astron. Astrophys.* **279,** 83-89 (1993)

16 Leppänen, K. J., Zensus, J. A. & Diamond, P. J. Linear polarization imaging with Very Long Baseline Interferometry at high frequencies. *Astron. J.* **110,** 2479-2492 (1995).

17 de Pater, I & Perley, R. A. The radio structure of 3C 279. *Astrophys. J.* **273,** 64-69 (1983).

18 Cotton, W. D., *et al.* 3C 279 - the case for superluminal expansion. *Astrophys. J.* **229,** L115-L117 (1979).

19 Blandford, R.D. & Königl, A. Relativistic jets as compact radio sources. *Astrophys. J.* **232,** 34-48 (1979).

20 Marscher, A. P. Accurate formulae for the self-Compton x-ray flux density from a uniform spherical compact radio source. *Astrophys. J.* **264,** 296-297 (1983).

21 Ghisellini, G., Padovani, P., Celotti, A. & Maraschi, L. Relativistic bulk motion in active galactic nuclei. *Astrophys. J.* **407,** 65-82 (1993).

22 Marscher, A. P. & Gear, W. K. Models for high-frequency radio outbursts in extragalactic

sources, with application to the early 1983 millimeter-to-infrared flare of 3C 273. *Astrophys. J.* **298,** 114-127 (1985).

23 Hughes, P. A., Aller, H. D. & Aller, M. F. Synchrotron emission from shocked relativistic jets. I - The theory of radio-wavelength variability and its relation to superluminal motion. *Astrophys. J.* **341,** 54-79 (1989).

24 Wardle, J. F. C., Cawthorne, T. V., Roberts, D. H. & Brown, L. F. Interpretation of VLBI kinematic and polarization data: application to 3C 345. *Astrophys. J.* **437,** 122-135 (1994).

25 Legg, M. P. C. & Westfold, K. C. Elliptic polarization of synchrotron radiation. *Astrophys. J.* **154,** 499-514 (1968).

26 Bicknell, G. V. in *Energy Transport in Radio Galaxies and Quasars* (eds. P. E. Hardee, A. H. Bridle & J. A. Zensus) 253-260 (A.S.P. Conference Series 100, Astronomical Society of the Pacific: San Fransisco, 1996).

27 Fanaroff, B. & Riley, J. M. The morphology of extragalactic radio sources of high and low luminosities. *Mon. Not. R. Astron. Soc.* **167,** 31P-36P (1974).

28 Duncan, G. C. & Hughes, P. A. Simulations of relativistic extragalactic jets. *Astrophys. J.* **436,** L119-L122 (1994).

29 Alexander, P. & Pooley, G. G. in *Cygnus A - Study of a Radio Galaxy* (eds. C. L. Carilli & D. E. Harris) 149-157 (Cambridge University Press: Cambridge, 1996).

30 Scheuer, P. A. G. in *Energy Transport in Radio Galaxies and Quasars* (eds. P. E. Hardee, A. H. Bridle & J. A. Zensus) 1-7 (A.S.P. Conference Series 100, Astronomical Society of the Pacific: San Fransisco, 1996).

31 Blandford, R. D. & Levinson, A. Pair cascades in extragalactic jets. 1: Gamma rays.

Astrophys. J. **441,** 79-95 (1995).

32 Marcowith A., Henri, G. & Pelletier, G. Gamma-ray emission of blazars by a relativistic electron-positron beam. *Mon. Not. R. Astron. Soc.* **277,** 681-699 (1995).

33 Mannheim, K. & Biermann, P. L. Gamma-ray flaring of 3C 279 - A proton-initiated cascade in the jet? *Astron. Astrophys.* **253,** L21-L24 (1992).

34 Bednarek, W. & Calvani, M. X- and gamma-ray emission from 3C 273. *Astron. Astrophys.* **245,** 41-47 (1991).

35 Burns, M. L. & Lovelace, R. V. E. Theory of electron-positron showers in double radio sources. *Astrophys. J.* **262,** 87-99 (1982).

36 Roberts, D. H., Wardle, J. F. C. & Brown, L. F. Linear polarization radio imaging at milliarcsecond resolution. *Astrophys. J.* **427,** 718-744 (1994).

37 Cotton, W. D. Calibration and imaging of polarization sensitive Very Long Baseline Interferometer observations. *Astron. J.* **106,** 1241-1248 (1993).

38 Wardle, J. F. C. & Roberts, D. H. in *Compact Extragalactic Radio Sources* (eds. J. A. Zensus & K. I. Kellermann) 217-222 (Workshop Proceedings, NRAO: Socorro, NM, 1994).

39 Homan, D. C., Ojha, R., Wardle, J. F. C. & Roberts, D. H. in *IAU Colloquium 164: Radio Emission from Galactic and Extragalactic Compact Sources* (eds. J. A. Zensus, G. B. Taylor & J. M. Wrobel) (in the press) (A.S.P. Conference Series, Astronomical Society of the Pacific: San Fransisco, CA, 1998).

This work has been supported by NSF and NASA. We thank Dr. Tom Jones for a careful reading of the manuscript.

Table 1: July 1996 component data on 3C 279

Component	r (mas)	Θ (deg)	ν (GHz)	I (Jy)	m_L (%)	χ (deg)	m_C (%)
CE	...	...	15	7.58	10.7	−83	...
			22	10.46	8.7	−84	...
CW	0.10	−112	15	9.19	9.9	19	1.0
			22	10.54	12.6	27	≤ 0.5
K3	0.86	−122	15	0.61	8.4	−25	< 2.2
			22	0.54	17.4	−8	...
K2	2.72	−119	15	0.85	2.6	55	< 1.6
			22	0.53	5.8	81	...
K1	3.06	−113	15	1.67	13.7	67	< 0.8
			22	1.66	13.9	67	...

Table 1: Component properties determined by model fitting in the u-v plane using the program DIFMAP. Component positions were determined from the 22 GHz data, and are given with respect to the component CE. Positions determined from the 15 GHz data are consistent with these, and show no significant shift in the position of CE with frequency. The linear polarization of each component was determined by solving for Stokes Q and U (using DIFMAP) at the positions given by the model fitting in total intensity.

Table 2: Two models for component CW

k	ϵ (deg)	ξ	δ	γ_{min}	Λ	m_L (%)	m_C (%)	τ_F	τ_C
0.6	20	0.3	20	15	1.00	9.2	0.89	1.38	1.37
				10	0.39	9.4	0.87	1.46	1.65
				5	0.06	9.8	0.96	1.20	2.08
				3	0.015	10.1	0.97	0.87	2.48
0.2	40	0.6	10	20	1.00	10.8	0.82	1.31	1.18
				12	0.27	10.2	0.92	1.30	1.52
				5	0.027	10.0	1.10	1.26	2.10
				3	0.006	10.5	1.00	0.83	2.44

Table 2: Table 2: Two models that reproduce the observed properties (m_L, m_C and τ_F) of component CW. In these models the underlying jet contains an isotropic tangled magnetic field of strength B_r and a uniform component of strength $B_u = \xi B_r$ aligned with the jet. The shock strength is described by the compression factor, k, where unit length is compressed to length k. The line of sight makes an angle ϵ with the plane of compression, in the frame of the radiating fluid, and δ is the Doppler factor. For each model, many combinations of γ_{min} and Λ can reproduce the observations. As γ_{min} decreases, Λ must become small to avoid producing excessive Faraday rotation (τ_F).

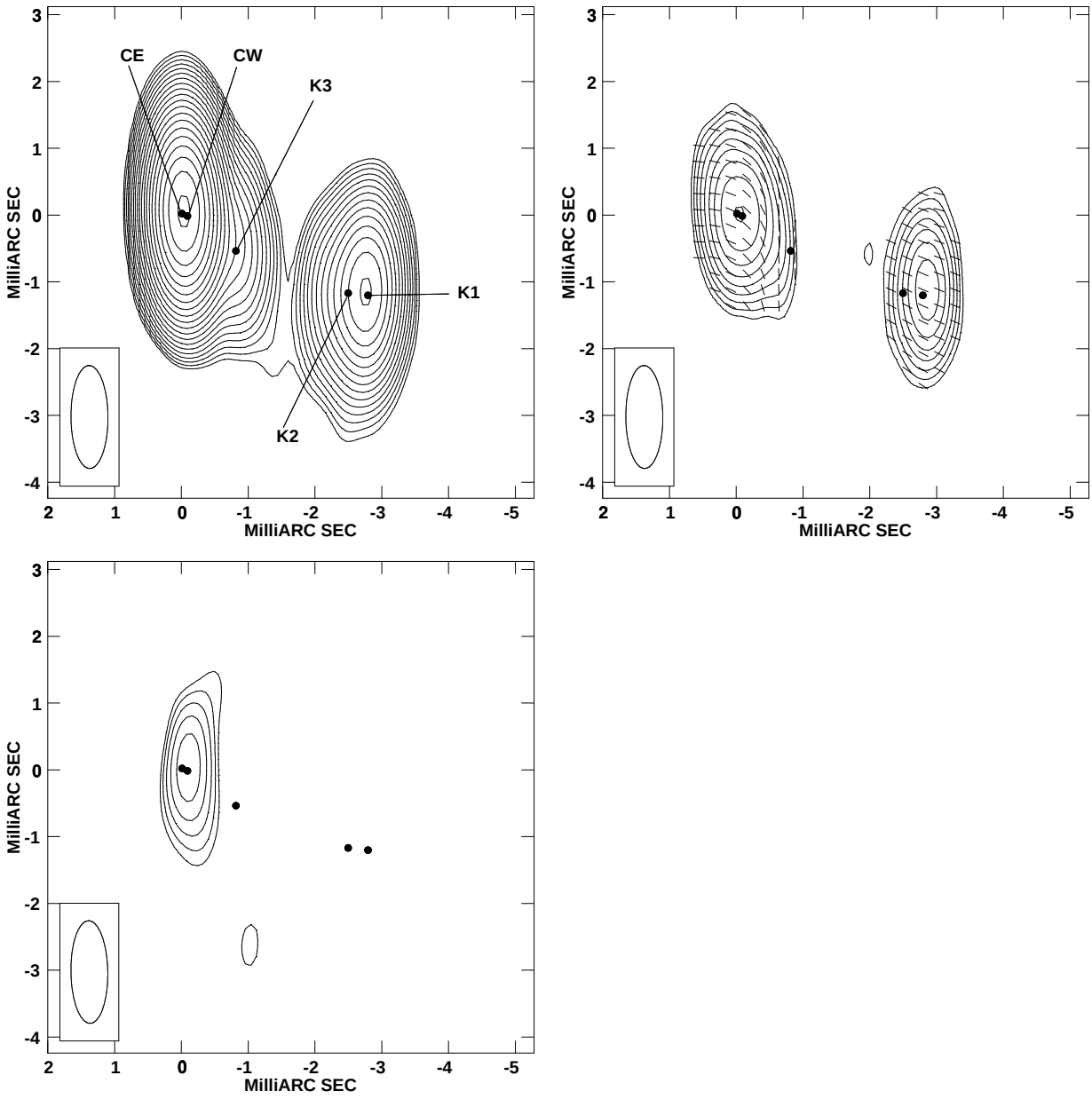

Fig. 1.— Caption on Following Page

Fig. 1.— Images of 3C 279 at 15.36 GHz, epoch July 1996. In each image the contour intervals are factors of $\sqrt{2}$, and the restoring beam is given by ellipse in the lower left corner. a) Total intensity image: the map peak is 15.40 Jy/beam, and the bottom contour is 0.02 Jy/beam. b) Linearly polarized intensity image with superimposed (electric) position angle vectors. The map peak is 0.325 Jy/beam, and the bottom contour is 0.02 Jy/beam. c) Circularly polarized intensity image (Stokes V): the map peak is 0.078 Jy/beam, and the bottom contour is 0.015 Jy/beam. The fitted model component positions are shown in each figure, and labeled in the first panel. The images display the familiar core-jet structure of 3C 279 (cf Leppänen *et al.* [16]), with a compact core to the east and a jet extending to the south west in position angle $-113°$. Model fitting in total intensity shows that the core consists of two closely spaced components of similar strength (components CE and CW). This is more easily seen in the linear polarization image, where the swing in the electric vectors clearly indicates the presence of two components. The bright knot (K1) at a distance of 3.0 mas from the core has a proper motion with respect to the core of 0.27 ± 0.04 mas/yr, corresponding to an apparent transverse velocity of $\beta_{app} = 8.0 \pm 1.2$.